

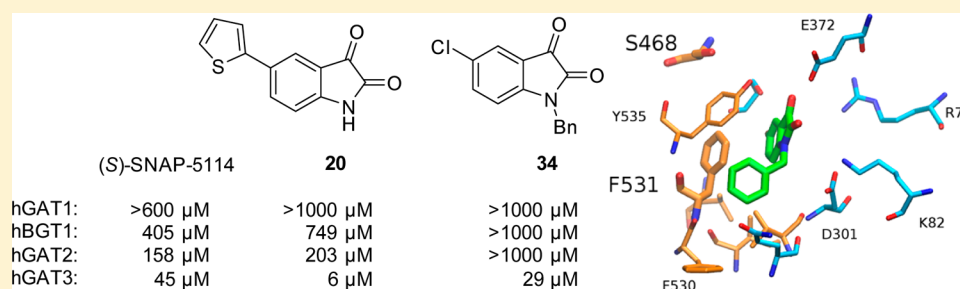
Identification of the First Highly Subtype-Selective Inhibitor of Human GABA Transporter GAT3

Maria Damgaard, Anas Al-Khawaja, Stine B. Vogensen, Andreas Jurik,[†] Maarten Sijm, Maria E. K. Lie, Mathias I. Bæk, Emil Rosenthal, Anders A. Jensen, Gerhard F. Ecker,[†] Bente Frølund, Petrine Wellendorph,* and Rasmus P. Clausen*

Department of Drug Design and Pharmacology, Faculty of Health and Medical Sciences, University of Copenhagen, Universitetsparken 2, DK-2100 Copenhagen, Denmark

[†]Department of Pharmaceutical Chemistry, University of Vienna, Althanstrasse 14, A-1090 Vienna, Austria

Supporting Information



ABSTRACT: Screening a library of small-molecule compounds using a cell line expressing human GABA transporter 3 (hGAT3) in a [³H]GABA uptake assay identified isatin derivatives as a new class of hGAT3 inhibitors. A subsequent structure–activity relationship (SAR) study led to the identification of hGAT3-selective inhibitors (i.e., compounds **20** and **34**) that were superior to the reference hGAT3 inhibitor, (S)-SNAP-5114, in terms of potency (low micromolar IC₅₀ values) and selectivity (>30-fold selective for hGAT3 over hGAT1/hGAT2/hBGT1). Further pharmacological characterization of compound **20** (5-(thiophen-2-yl)indoline-2,3-dione) revealed a noncompetitive mode of inhibition at hGAT3. This suggests that this compound class, which has no structural resemblance to GABA, has a binding site different from the substrate, GABA. This was supported by a molecular modeling study that suggested a unique binding site that matched the observed selectivity, inhibition kinetics, and SAR of the compound series. These compounds are the most potent GAT3 inhibitors reported to date that provide selectivity for GAT3 over other GABA transporter subtypes.

KEYWORDS: GABA uptake, inhibitor, hGAT3 selective, noncompetitive, kinetics, isatin

The major inhibitory neurotransmitter in the central nervous system, γ -aminobutyric acid (GABA) (**1**, Figure 1), plays a central role in normal brain function, and it has been demonstrated that abnormalities in GABAergic neurotransmission in the brain can lead to several disorders. Proteins involved in GABA neurotransmission are, therefore, interesting therapeutic targets, and compounds perturbing this system in a selective manner are considered to be drug candidates for a number of diseases.¹ For example, epileptic and sleep disorders are treated with compounds acting at the GABAergic system, mainly by increasing GABAergic neurotransmission. An important part of the GABAergic system is the uptake of GABA into neurons and glial cells mediated by GABA transporters (GATs), and inhibition of this transport has been shown to be effective in the treatment of seizures in epileptic disorders.² Its therapeutic relevance has been demonstrated by the GABA uptake inhibitor tiagabine (Gabitril) (**2**), which is a clinically approved drug used as add-on therapy for partial epilepsy.

Four different mammalian GABA transporters have been cloned, named GAT1, GAT2, GAT3, and BGT1 according to the IUPHAR nomenclature. GAT1 is the most studied transporter due to the existence of highly potent and specific inhibitors, such as tiagabine (**2**).³ Development of highly selective compounds toward the other GABA transporters has been limited. GAT1 and GAT3 are exclusively present in the brain, although they exhibit a heterogeneous distribution, primarily in neurons (GAT1) and astrocytes (GAT3).⁴ By contrast, BGT1 and GAT2 are also expressed in other organs, and, although their expression levels in the brain are debated,^{5,6} the role of BGT1 in relation to GABAergic neurotransmission is supported by the anticonvulsant effect of the mixed GAT1/BGT1 inhibitor (*RS*)-4-[*N*-[1,1-bis(3-methyl-2-thienyl)but-1-en-4-yl]-*N*-methylamino]-4,5,6,7-tetrahydrobenzo[*d*]isoxazol-3-ol (EF1502, **3**)⁷ and a

Received: May 28, 2015

Revised: June 23, 2015

Published: July 8, 2015

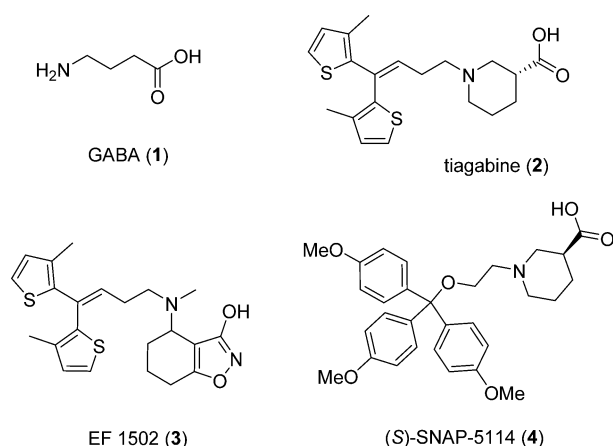


Figure 1. Structures of γ -aminobutyric acid (GABA, 1), the highly GAT1 selective inhibitor tiagabine (2), EF 1502 (3), a mixed BGT1/GAT1 inhibitor, and the moderately potent GAT3 inhibitor (S)-SNAP-5114 (4).

proposed role of BGT1 in regulating extrasynaptic GABA neurotransmission.⁸ Much still remains to be learned about these transporter subtypes, but this requires more selective compounds.

Due to its exclusive expression in the brain and primary localization in astrocytes, GAT3 is a very interesting subtype and is of potential clinical relevance in epilepsy and stroke,^{4,9} but a role for GAT3 in neurons has also been demonstrated in some studies.^{10,11} Although (S)-SNAP-5114 (4) is often applied as a

selective GAT3 inhibitor, the selectivity of the compound, and of several synthesized analogues,¹² is not sufficiently pronounced to exclude effects on other GABA transporter subtypes. In addition, (S)-SNAP-5114 has limited brain uptake and modest chemical stability, thus limiting its use *in vivo*.¹³ Consequently, there is a need to develop more selective GAT3 inhibitors that can be used to probe the physiological roles and therapeutic potential of this transporter.

The GABA transporters belong to superfamily 6 of solute carriers (SLC6), which are Na^+/Cl^- -dependent neurotransmitter transporters that share a common topology of 12 transmembrane (TM) spanning segments. Biochemical and X-ray crystallographic studies of members of this transporter family have provided knowledge on their mechanism of transport. Currently, GABA is believed to be transported according to an alternate access model of substrate translocation, where GABA and cotransported ions are assumed to enter a central binding site from the extracellular space in an outward-open state of the transporter, followed by transition to a state where GABA is occluded. Subsequently, an inward-facing conformation of the protein arises that has lower substrate affinity, which triggers the release of the substrate into the cell.¹⁴ Although it is still debated, it has been proposed that a secondary substrate binding site (S2) exists at the extracellular part of the occluded state that needs to be occupied to induce transport.^{15,16} Currently, most of the known inhibitors of the GABA reuptake system display competitive inhibition at the central substrate binding site, but compounds with a noncompetitive profile have also been described.¹⁷ Biostructural studies have enabled comparisons of aligned GAT homology models to be made, on the basis of the

Table 1. Pharmacological Characterization of GABA (1), (S)-SNAP-5114 (4), and a Number of Commercially Available Isatin Analogues at the Four Human GAT Subtypes*

compd	R ₁	R ₂	R ₃	R ₄	R ₅	IC ₅₀ (μM) (pIC ₅₀ \pm SEM)				GAT3/1 selectivity ratio
						hGAT1	hBGT1	hGAT2	hGAT3	
GABA (1)						2.5 (5.60 \pm 0.04)	5 (5.29 \pm 0.02)	2.2 (5.71 \pm 0.14)	1.4 (5.87 \pm 0.05)	1.8
(S)-SNAP-5114 (4)						>600 ^c	405 (3.40 \pm 0.05)	158 (3.81 \pm 0.06)	45 (4.37 \pm 0.10)	>13.3
5	H	H	Br	F	H	541 ^a (3.27 \pm 0.05)	55 ^b (4.26 \pm 0.02)	65 ^b (4.19 \pm 0.05)	108 ^a (4.00 \pm 0.07)	5.0
6	H	H	Cl	H	H	199 (3.72 \pm 0.08)	146 (3.83 \pm 0.03)	223 (3.66 \pm 0.06)	18 (4.78 \pm 0.09)	11
7	H	H	Cl	H	Cl	114 (3.98 \pm 0.10)	55 (4.26 \pm 0.02)	76 (4.14 \pm 0.08)	17 (4.80 \pm 0.08)	6.7
8	H	H	Cl	H	Me	1080 ^a (3.13 \pm 0.28)	27 ^b (4.56 \pm 0.01)	105 ^b (4.04 \pm 0.16)	18 ^b (4.78 \pm 0.09)	60
9	H	H	OCF ₃	H	H	181 (3.75 \pm 0.04)	47 (4.33 \pm 0.03)	51 (4.30 \pm 0.03)	16 (4.79 \pm 0.05)	11
10	H	H	iPr	H	H	218 (3.67 \pm 0.04)	155 (3.81 \pm 0.04)	174 (3.76 \pm 0.03)	25 (4.72 \pm 0.18)	8.7
11	H	H	NO ₂	Me	Me	229 (3.64 \pm 0.01)	250 (3.60 \pm 0.03)	266 (3.58 \pm 0.04)	55 (4.38 \pm 0.17)	4.2
12	Cl	H	H	H	H	363 (3.46 \pm 0.09)	130 (3.90 \pm 0.08)	200 (3.70 \pm 0.05)	22 (4.67 \pm 0.08)	17
13	H	H	I	H	H	46 ^b (4.34 \pm 0.06)	21 ^b (4.70 \pm 0.07)	28 ^b (4.58 \pm 0.08)	9 (5.06 \pm 0.02)	5.1
14	H	Cl	Cl	H	H	85 (4.07 \pm 0.03)	54 (4.27 \pm 0.04)	109 (3.97 \pm 0.05)	10 (5.01 \pm 0.11)	8.5

*Compounds were tested for their ability to inhibit uptake of 30 nM [³H]GABA at the four human GAT subtypes stably expressed in CHO cells. IC₅₀ values were determined by curve-fitting analysis. Compounds were selected based on their ability to inhibit hGAT3 at a 50 μM concentration (Supporting Information Figure S1). All data points were determined in triplicate and repeated in at least three independent experiments. ^aThe compounds displayed less than 90% but more than 50% inhibition, and the concentration–inhibition curves were accordingly fitted to the value of 100% inhibition (3 mM GABA). ^bThe bottom plateaus of the fitted curves were less than the GABA maximal inhibition plateau (set to 100%) and consequently gave the following relative maximum inhibition levels (% inhibition \pm SD): hGAT1: 13, 53 \pm 4; hBGT1: 5, 60 \pm 5; 8, 69 \pm 2; 13, 79 \pm 4; hGAT2: 5, 60 \pm 8; 8, 61 \pm 7; 13, 72 \pm 8; hGAT3: 8, 87 \pm 5. ^cThe compound displayed less than 50% inhibition, and the IC₅₀ value was accordingly estimated as being greater than the highest tested concentration.

crystal structures of the homologous bacterial leucine transporter LeuT and the *Drosophila melanogaster* dopamine transporter (DAT),^{18,19} which offers the possibility of investigating potential subtype-selective binding cavities. Combining knowledge of the steric demands of the inhibitor molecules and sequence differences facilitates docking studies for the generation of binding hypotheses.

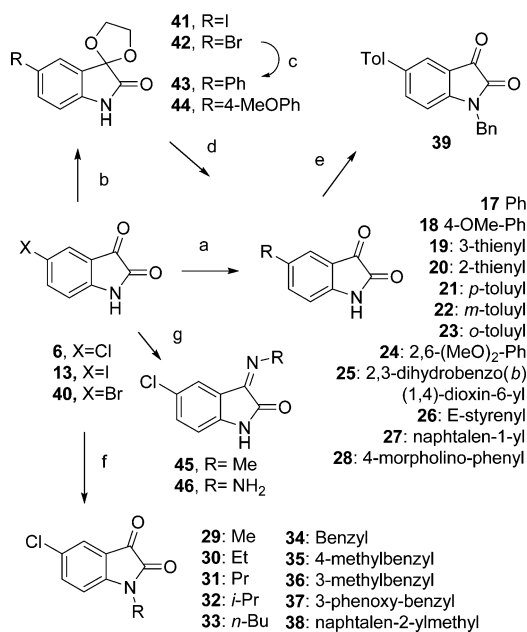
In the current study, we report the development of a new structural class of highly subtype-selective hGAT3 inhibitors that work in a noncompetitive manner, possibly by acting at a new binding pocket for inhibition of GABA transporters.

RESULTS AND DISCUSSION

A commercial compound library consisting of 4000 structurally diverse compounds (Enamine, Monmouth, NJ, USA) was screened for its ability to inhibit the uptake of 30 nM [³H]GABA into Chinese hamster ovary (CHO) cells stably expressing the human GAT3 (hGAT3) subtype.²⁰ Bromo-/fluoro-substituted isatin **5** (Table 1) was identified as a hGAT3 inhibitor, thus representing a new structural scaffold among GABA uptake inhibitors bearing no structural resemblance to GABA. An extended characterization of commercially available analogues of **5** was performed as an initial structure–activity relationship (SAR) study. Forty eight commercially available isatin analogues were tested in the [³H]GABA uptake assay at the hGAT3-CHO cell line in a single concentration. The structures of the 48 analogues and the results from this follow-up screening are presented in Figure S1, Supporting Information. From this screening, nine compounds (**6–14**, Table 1) showed inhibition to a greater degree than that with the original hit (**5**) at hGAT3 and were consequently selected for further characterization at CHO cell lines expressing each of the four human GAT subtypes: hGAT1, hBGT1, hGAT2, and hGAT3. Concentration–inhibition curves were generated for each of the compounds, and the estimated IC₅₀ values are presented in Table 1. The initial screening hit (**5**) displayed an inhibitory potency for hGAT3 of 108 μM and an hGAT3/1 selectivity ratio of 5; however, it did not discriminate among hBGT1, hGAT2, and hGAT3. Compounds with a small lipophilic substituent in the R₃ position (**6**, **10**, and **13**) displayed both higher hGAT3 potency and hGAT3/1 selectivity, whereas compounds lacking a substituent in the R₃ position were weaker inhibitors at hGAT3. Moving the halogen to positions R₂, R₄, and R₅ completely abolished hGAT3 inhibition. The N-methylated compound (**11**) did not display more potent inhibition than that of the original hit, whereas the N-chloro compound (**12**) improved both hGAT3 potency and hGAT3/1 selectivity. Thus, activities of this scaffold responded well to the changes in substituents, and there seemed to be room for improvement of both hGAT3 potency and hGAT3/1 selectivity. On the basis of these findings, a series of compounds with different R₁ and R₃ substituents was designed to investigate critical areas for GAT3 inhibition and selectivity further. In particular, we wanted to explore how larger substituents in the R₃ position and on the ring nitrogen would affect the GAT3 selectivity observed in the initial SAR.

The procedures for the synthesis of compounds **15–39** are depicted in Scheme 1. 5-Alkyl-substituted analogues **15** and **16** were synthesized via the Sandmeyer isonitrosoacetanilide isatin synthesis as previously described.²¹ The reaction was not applicable for the 5-aryl-substituted analogues. Instead, these analogues were synthesized via the Suzuki cross-coupling reaction.²² Conditions previously described for Suzuki reactions on iodoisatins were tested.^{23,24} However, low yields were

Scheme 1. Synthesis of 17–46^a



^aReagents and conditions: (a) R-B(OH)₂, Pd(dppf)Cl₂, NaHCO₃, DME, H₂O, heating, 2–12%; (b) ethylene glycol, PTSA (*p*-toluenesulfonic acid), toluene, reflux, 68%; (c) Ph-B(OH)₂ or *p*-OMe-Ph-B(OH)₂, Pd(PPh₃)₄ or Pd(dppf)Cl₂, NaHCO₃, DME, H₂O, heating, 41–94%; (d) conc. HCl, MeOH, 80 °C; (e) Bn-Br, K₂CO₃, DMF, microwave heating, 85%; (f) R-I or R-Br, K₂CO₃, DMF, microwave heating, 20–65%; (g) hydrazin or MeNH₂.

obtained when coupling 5-iodo or 5-bromoisatin under the described conditions. This has previously been described in cross-coupling reactions of isatins.²³ Ketal protection of the free carbonyl group was attempted to optimize the yields.²³ 5-Iodoisatin (**13**) and 5-bromoisatin (**40**) were refluxed with ethylene glycol and catalytic amounts of *p*-toluenesulfonic acid in toluene to yield ketal-protected compounds **41** and **42**. Ketal-protected isatins **41** and **42** were cross-coupled with phenylboronic acid and (4-methoxyphenyl)boronic acid using previously reported conditions,²⁵ affording **43** and **44**. Deprotection of the ketal moiety in concentrated aqueous hydrochloric acid gave desired compounds **17** and **23**; however, their yields were low. The overall yield of the Suzuki reactions did not differ substantially between the protected and unprotected isatins; hence, the unprotected reaction was preferred. A number of 5-aryl-substituted analogues was synthesized using 5-iodoisatin directly in Suzuki cross-coupling reactions, giving compounds **19–28**. N-Alkylated analogues **29–39** were obtained using the alkyl halide and potassium carbonate in DMF under microwave heating in fair yields.

All synthesized analogues were assayed at all four hGAT subtypes in the [³H]GABA uptake assay, and the results are presented in Table 2. Substitution of the isatin scaffold in the R₃ position with small aliphatic substituents (**15** and **16**) yielded IC₅₀ values of 49 and 15 μM at hGAT3 and an hGAT3/1 selectivity of 11 and 16, respectively. Increasing the size of the substituents in this position to larger aromatic substituents (**17** and **19–23**) increased the inhibitory potency at hGAT3 further, as these analogues exhibited IC₅₀ values in the low micromolar range and higher hGAT3/1 selectivity ratios (>29 or higher). In contrast, substitution of the distal aryl with groups larger than a methyl (**18** and **24–28**) led to complete loss of activity. For the

Table 2. Structure–Activity Relationships of Isatin Analogues at the Four Human GAT Subtypes*

IC₅₀ (μM) (pIC₅₀ ± S.E.M)

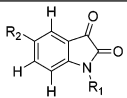
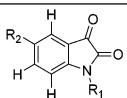
cmpd	R ₁	R ₂	IC ₅₀ (μM) (pIC ₅₀ ± S.E.M)				GAT3/1 selectivity ratio
			hGAT1	hBGT1	hGAT2	hGAT3	
							
15	H	Et	532 ^a (3.27±0.01)	680 ^a (3.17±0.03)	643 ^a (3.20±0.06)	49 (4.34±0.12)	11
16	H	Sec-Bu	233 ^a (3.67±0.13)	100 (4.01±0.08)	171 (3.77±0.03)	15 (4.84±0.10)	16
17	H	Ph	876 ^b (3.07±0.07)	314 ^c (3.64±0.27)	63 ^c (4.24±0.13)	8 (5.09±0.09)	110
18	H	4-Ome-Ph	>1000	>1000 ^b	N.A.	>1000 ^b	-
19	H	3-thienyl	>1000	33 ^c (4.48±0.003)	50 ^c (4.32±0.02)	17 ^c (4.79±0.11)	>59
20	H	2-thienyl	>1000	749 ^c (3.21±0.19)	203 ^c (3.74±0.14)	6 ^c (5.20±0.05)	>167
21	H	<i>p</i> -toluyl	>1000	>1000 ^b	N.A.	22 ^c (4.66±0.05)	>45
22	H	<i>m</i> -toluyl	>1000	55 ^c (4.26±0.003)	63 ^c (4.20±0.002)	35 ^c (4.47±0.08)	>29
23	H	<i>o</i> -toluyl	>1000	50 ^c (4.30±0.02)	52 ^c (4.29±0.02)	24 ^c (4.63±0.09)	>42
24	H	2,6-Ome-Ph	N.T.	N.T.	N.T.	>300 ^b	-
25	H	(2,3-di-hydrobenzo [b][1,4]-dioxin-6-yl)	N.T.	N.T.	N.T.	>300 ^b	-
26	H	(<i>E</i>)- styrenyl	N.T.	N.T.	N.T.	>300 ^b	-
27	H	naphtalen-1-yl	N.T.	N.T.	N.T.	>300 ^b	-
28	H	4-morpholino-phenyl	N.T.	N.T.	N.T.	>300 ^b	-
29	Me	Cl	906 ^a (3.04±0.03)	533 ^a (3.28±0.04)	421 ^a (3.39±0.07)	232 ^a (3.67±0.11)	3.9
30	Et	Cl	563 ^a (3.25±0.01)	453 ^a (3.35±0.05)	453 ^a (3.35±0.05)	124 (3.96±0.15)	4.5
31	nPr	Cl	248 ^a (3.61±0.03)	198 (3.71±0.04)	198 (3.71±0.04)	52 (4.31±0.12)	4.8
32	iPr	Cl	464 ^a (3.34±0.04)	235 ^a (3.63±0.02)	235 ^a (3.63±0.02)	46 (4.40±0.16)	10

Table 2. continued

cmpd	R ₁	R ₂	IC ₅₀ (μM) (pIC ₅₀ ± S.E.M)				GAT3/1 selectivity ratio
			hGAT1	hBGT1	hGAT2	hGAT3	
							
33	nBu	Cl	184 (3.74±0.04)	140 (3.86±0.05)	140 (3.86±0.05)	53 (4.28±0.05)	3.5
34	Bn	Cl	>1000	>1000	>1000	29 ^c (4.65±0.18)	>34
35	4-MeBn	Cl	N.T.	N.T.	N.T.	>1000 ^b	-
36	3-MeBn	Cl	N.T.	N.T.	N.T.	>300 ^b	-
37	Naphtalen-2-ylmethyl	Cl	N.T.	N.T.	N.T.	>300 ^b	-
38	3-phenoxy-benzyl	Cl	N.T.	N.T.	N.T.	>300 ^b	-
39	Bn	<i>p</i> -toluyl	N.T.	N.T.	N.T.	>1000 ^b	-
45		R=Me	N.T.	N.T.	N.T.	>1000 ^b	-
46		R=NH ₂	N.T.	N.T.	N.T.	>1000 ^b	-

*Compounds were tested for their ability to inhibit uptake of 30 nM [³H]GABA at the four human GAT subtypes stably expressed in CHO cells. IC₅₀ values were determined by curve-fitting analysis and are based on at least three independent experiments, whereas compounds with no activity are based on at least two independent experiments. All data points were carried out in triplicate. N.T., not tested. ^aThe compounds displayed less than 90% but more than 50% inhibition, and the concentration–inhibition curves were accordingly fitted to the value of 100% inhibition (3 mM GABA). ^bThe compounds displayed less than 50% inhibition, and the IC₅₀ values were accordingly estimated as being greater than the highest tested concentration. ^cThe bottom plateaus of these fitted curves were less than the GABA maximal inhibition plateau (set to 100%) and consequently gave the following relative maximum inhibition levels (% inhibition ± SD): hBGT1: 17, 62 ± 9; 19, 50 ± 11; 20, 36 ± 14; 22, 63 ± 9; 23, 61 ± 6; hGAT2: 17, 78 ± 7; 19, 47 ± 21; 20, 66 ± 7; 22, 58 ± 17; 23, 52 ± 14; hGAT3: 19, 80 ± 10; 20, 90 ± 2; 21, 73 ± 1; 22, 81 ± 8; 23, 83 ± 8; 34, 43 ± 11.

N-substituted compounds, small substituents in the R₁ position (29, 30) impaired potency for hGAT3; however, potency was regained for larger substituents (31–33), and the R₁ benzyl-substituted compound 34 displayed an hGAT3 IC₅₀ value of 29 μM and an hGAT3/1 ratio greater than 100. Substitution on the R₁ benzyl group was detrimental to the activity of the compounds, as the combination of an aryl group in the R₃ position and a benzyl in the R₁ position (39) completely abolished activity.

As can be seen from Tables 1 and 2, a number of the isatin analogues displayed partial inhibition of [³H]GABA uptake at their saturating concentrations. This phenomenon was seen in the concentration–inhibition curves as a bottom plateau less than the control value of 100% inhibition with 3 mM GABA. An example of such a curve is shown in Figure 2A for 34 at hGAT3. For comparison, the concentration–inhibition curves for isatin analogues 17 and 20 as well as reference compound (S)-SNAP-5114 (4), which all displayed full uptake inhibition, are also included in Figure 2. Several of the isatin analogues (e.g., 34 at hGAT3, Figure 2A) displayed partial inhibition of [³H]GABA uptake with apparent plateaus ranging from 36 to 90% of control, a phenomenon reported previously for the dopamine transporter.²⁶ Whether the observed partial behavior of some isatin analogues is related merely to intrinsic pharmacological/

structural properties of the compounds or to physicochemical properties, such as aggregation or reaching the solubility limits of the compounds at higher concentrations, is currently unclear. Clearly, solubility limits could mask either a full inhibition or a potential biphasic concentration–inhibition curve. The latter could exist if a compound binds with distinct affinities to two sites within the same transporter monomer or with different affinities to two monomers of a transporter dimer. An example of biphasic uptake kinetics has been reported for the dopamine transporter,²⁷ and dimerization of GATs has been reported for rat GAT1.²⁸

Figure 2B highlights the pronounced hGAT3 over hGAT1 subtype selectivity of compound 20 (more than 167 times) and demonstrates that 20 is more potent than (S)-SNAP-5114 (4) (data summarized in Tables 1 and 2). In addition, compound 20 showed an hGAT3 selectivity of at least 30-fold over the other GAT subtypes, whereas this is approximately 3-fold for (S)-SNAP-5114 (4). As described earlier, (S)-SNAP-5114 (4) has limited use *in vivo* due to its limited brain uptake and modest chemical stability.¹³

In addition to investigating the inhibitory activity of the synthesized compounds at the four hGATs, the mechanism underlying the inhibition of GAT3 transport exerted by 20 was further investigated by measuring the transport rate of

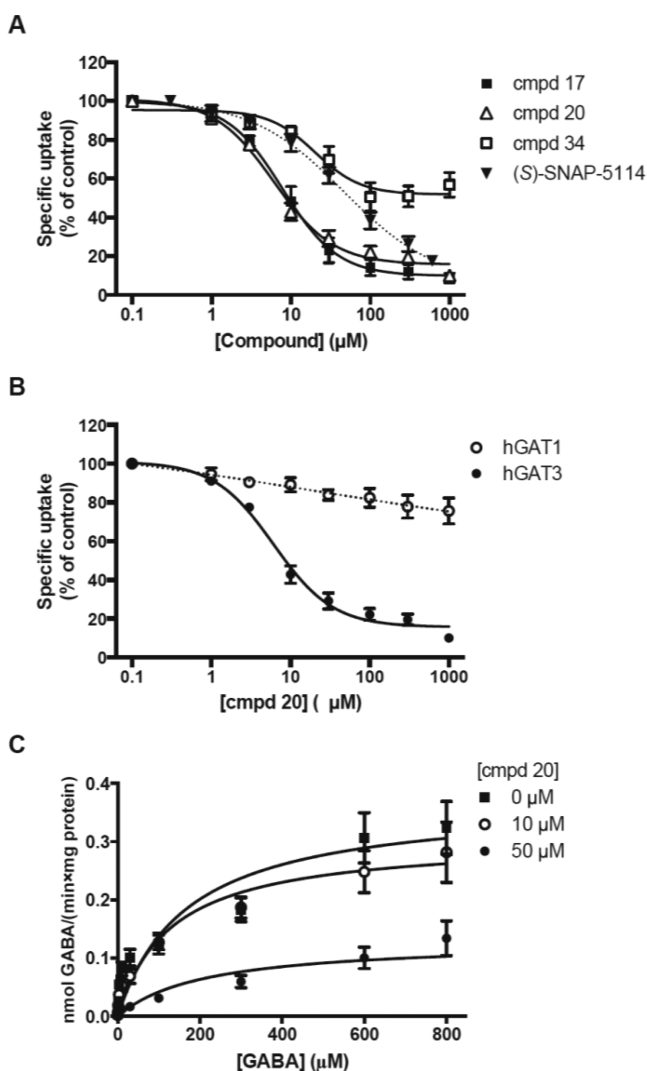


Figure 2. Pharmacological characterization of novel isatin analogues at hGATs stably expressed in CHO cells. (A) Concentration–inhibition curves for 17, 20, 34, and (S)-SNAP-5114 (4) at hGAT3. 34 displayed partial inhibition of [^3H]GABA uptake. The responses are normalized mean values of at least three independent experiments \pm SEM (see Tables 1 and 2 for mean IC_{50} values). (B) Concentration–inhibition curves for compound 20 at hGAT1 and hGAT3. The responses are normalized mean values of three independent experiments \pm SEM. Estimated IC_{50} value at hGAT1 is $>1000 \mu\text{M}$ and at hGAT3 is $6 \mu\text{M}$ (Table 2). (C) Effect of compound 20 on the GABA transport velocity through hGAT3. Specific transport velocity of increasing concentrations of GABA was measured in the [^3H]GABA uptake assay. The maximum concentration of [^3H]GABA was 100 nM. Data are given as nanomoles of GABA transported per minute and normalized to protein amount per well. Results are mean values of three independent experiments \pm SEM. The K_m values expressed in micromolar ($pK_m \pm \text{SEM}$) were estimated to be 0 μM 20, 172 (3.77 ± 0.03); 10 μM 20, 201 (3.82 ± 0.24); 50 μM 20, 246 (3.65 ± 0.13). The V_{max} values expressed as nanomoles of GABA/(min·mg protein) \pm SEM were estimated to be 0 μM 20, 0.39 ± 0.06 ; 10 μM 20, 0.28 ± 0.04 ; 50 μM 20, 0.13 ± 0.01 (the V_{max} value was constrained to the average of the maximal level). The V_{max} value in the presence of 50 μM 20 was significantly decreased compared to control, but no significant difference in pK_m was observed (one-way ANOVA followed by Dunnett's test; $P < 0.01$).

[^3H]GABA in the absence and presence of different fixed concentrations of compound 20. The results are shown in Figure 2C. Increasing the concentration of 20 resulted in a statistically

significant decrease in V_{max} whereas the pK_m value was not significantly altered. This suggested that compound 20 inhibits the uptake of GABA through hGAT3 in a noncompetitive manner. Kinetics studies were also performed for the structurally related compound 6, showing the same kinetics profile and thereby confirming a noncompetitive inhibition mode for the isatin analogues (results not shown). A noncompetitive inhibition mode for these compounds is not surprising because they show no structural resemblance to GABA.

A molecular modeling study was employed to suggest potential inhibitory binding sites for the compounds in the transporter that would be in accordance with the observed SAR and subtype selectivity of the compounds. Cavity analysis of comparative models for all subtypes revealed a potential site in an outward-open state of GAT3 between TM domains 10 and 11, containing residues on positions 10.49 (S468) and 11.60 (F531) (generic numbering according to Beuming et al.;²⁹ see Figure 3

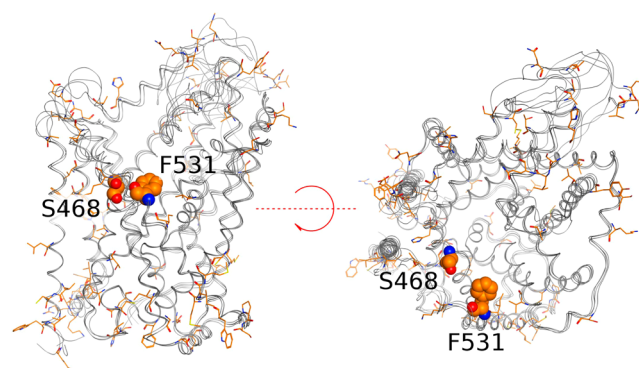


Figure 3. Localization of GAT3-selective residues (orange). Amino acids 10.49 (S468) and 11.60 (F531) located in the putative pocket are depicted in van der Waals surface.

and alignment in Figure S2, Supporting Information) that are not conserved in the three other human GATs. As can be seen in Figure 3, substrates could still enter the central binding cavity; additionally, the disputed secondary substrate binding site S2 is accessible. Thus, a noncompetitive mode of inhibition could root from impaired TM rearrangement needed for substrate translocation to the intracellular space.

Placement of the isatin derivatives into this site using a flexible docking workflow indicated a possible binding mode, which is in line with the SAR. For selected compounds, short molecular dynamics simulations in a membrane environment were performed to explore solvent-mediated interactions with surrounding residues.

The hydrophobic side of the compounds was mainly accommodated in the hydrophobic part of the pocket. An aromatic residue in position 10.64, which is present in all subtypes except hGAT1, was observed to support hydrophobic interactions with aromatic substituents in the 1- or 5-position, supporting the selectivity trends of the data set, as exemplified by compounds 17–23 and 34. The position of the polar oxo groups seem to be stabilized by a complex water-mediated hydrogen-bond network, occasionally involving polar residues of TM1, TM6, and the extracellular loop EL4. The fragile character of this network is underlined by the inactivity of compounds 45 and 46, which are substituted at the position of the 3-oxo group.

As exemplified by hGAT1 and hGAT3 in Figure 4, similar initial ligand placements could be observed for all four hGAT subtypes, but non-hGAT3 complexes were significantly less

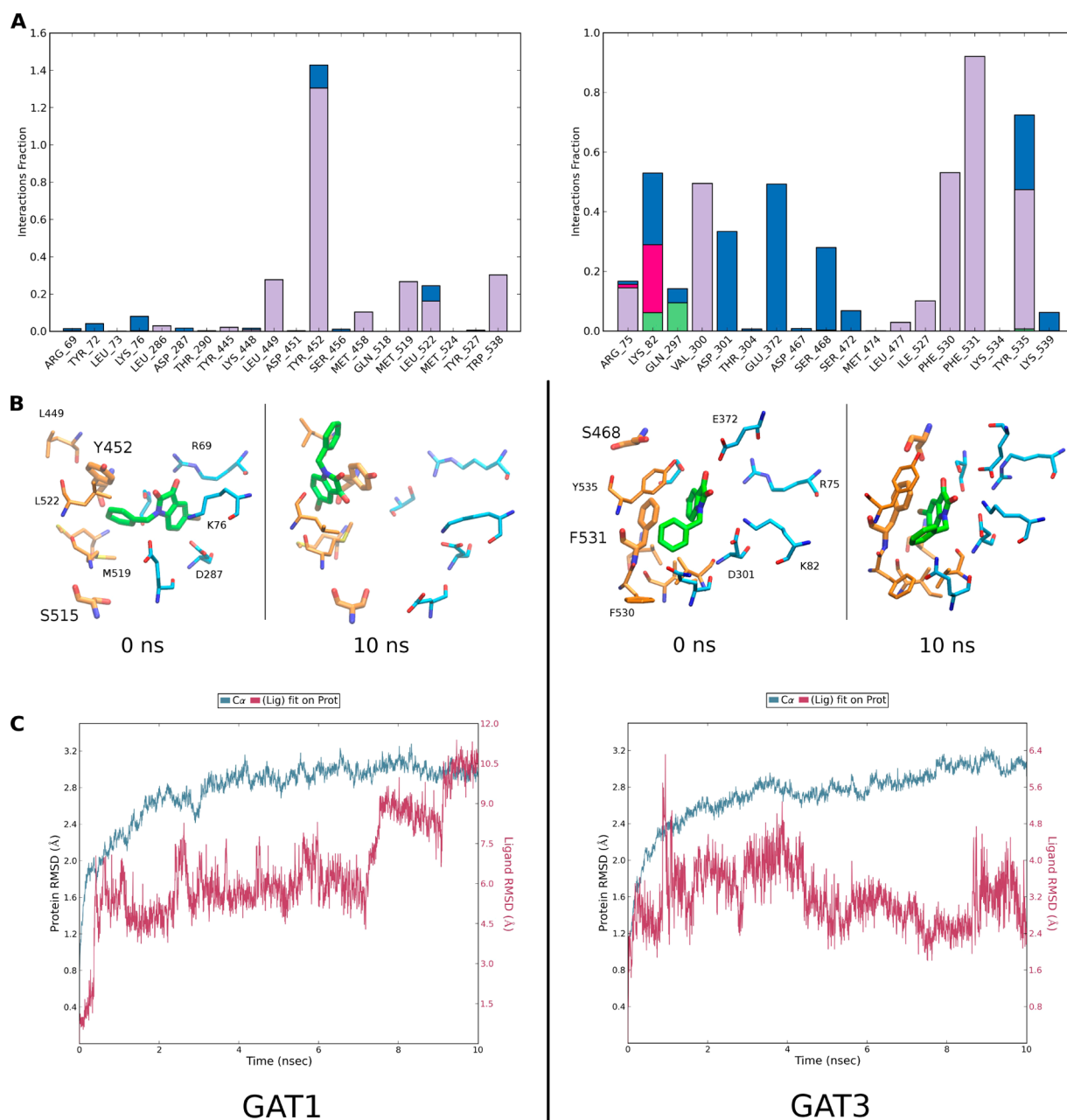


Figure 4. Molecular dynamics behavior of **34** at hGAT1 and hGAT3. (A) Protein–ligand contacts over the trajectory. Hydrophobic contacts are depicted in purple, hydrogen bonds, in green, ionic bonds, in pink, and water bridges, in blue. (B) Ligand position relative to key residues at the beginning and end of the simulation. (C) Protein (blue) and ligand (purple) root-mean-squared deviation (RMSD).

stable and displayed pronounced drifting of the ligands in the short molecular dynamics simulations. This underlines the importance of hydrophobic properties, as residues 10.49 (Y/Y/Y/S) and 11.60 (S/S/S/F) are, albeit switched, nearly identical for all of the GAT subtypes. Hence, the small difference of a phenolic hydroxyl group could cause the particular pharmacological properties of the data set.

Herein, we have reported the design, synthesis, and pharmacological evaluation of a new type of hGAT3-selective inhibitors based on the isatin scaffold. Compound **20** is a more potent analogue than the reference GAT3 inhibitor, (*S*)-SNAP-5114 (**4**), and its selectivity for hGAT3 compared to the other subtypes is significantly improved. Thus, selectivity for hGAT3 over hGAT2 and hBGT1 is increased from 3.5- and 9-fold to 34- and 124-fold, respectively. Some of the compounds display

partial inhibition of GABA transport. Interestingly, these compounds were shown to have a noncompetitive inhibition mode at hGAT3, which, together with the lack of structural resemblance to GABA, suggests a different binding site than that of previous inhibitors. Many of the previous GABA uptake inhibitors bear amino and acid groups, suggesting a binding site partially overlapping with GABA. A molecular modeling study evaluated potential binding sites in a full range of GABA transporter homology models, and only one binding site had the size and physiochemical characteristics that were in accordance with the observed potency and selectivity trends, which awaits further experimental validation. This is part of future studies that will also be directed at determining the blood–brain barrier permeability of selected analogues. Also, studies on the effect of compound **20** at neurons and astrocytes under normal and

diseased conditions, as well as how it could influence synaptic vesicle recycling and transporter exo/endocytosis, are of high importance. In conclusion, we have presented a new class of hGAT3-selective compounds that can be used as tool compounds to understand the pharmacology of hGAT3 and its involvement in disease.

METHODS

Chemistry. General Procedures. All anhydrous reactions were carried out in oven-dried glassware, under nitrogen. Solvents were of chromatography grade and dried using an SG Water solvent purification system (DCM, DMF, and THF) or with 3 Å molecular sieves. Commercially obtained chemicals were used without further purification. TLC was carried out on Merck precoated silica gel 60 F₂₅₄ plates and visualized using UV (254 nm). Column purifications were carried out manually using silica gel: 40–63 μm. NMR spectra were recorded on a 400 or 600 MHz Bruker Avance instrument. Data are reported as follows: chemical shift, multiplicity (s = singlet, d = doublet, dd = double doublet, t = triplet, bs = broad singlet, m = multiplet), integration, and coupling constants (Hz). Chemical shifts are reported in ppm, with the solvent resonance resulting from incomplete deuteration as the internal reference (CHCl₃ in CDCl₃: δ 7.26; (CH₃)₂SO in (CD₃)₂SO: δ 2.50), with the exception being samples in D₂O, to which 40 μL of dioxane per 100 mL of D₂O was added as reference (dioxane in D₂O: δ 3.75). Analytical HPLC was performed on a Merck-Hitachi HPLC system consisting of an L-7100 pump, an L-7200 autosampler, and an L-7400 UV detector (254 nm), using an Chromolith SpeedROD RP-18 column (4.6 × 50 mm) eluted at a flow rate of 4.0 mL/min. A linear gradient elution was performed with eluent A (H₂O/TFA 100:0.1) containing 0% solvent B (MeCN/H₂O/TFA, 90:10:0.01) increasing to 100% B over 5 min. Data were acquired and processed using the EZChrom Elite Software, version 3.1.7, by Hitachi. HPLC purity is ≥95%, unless otherwise stated. LC-MS method A: LC-MS was performed using an Agilent 1100 HPLC system with a XBridge 3.5 μm C18 column (100 × 4.6 mm) using gradient elution from buffer A (H₂O/CH₃CN/HCOOH, 95:5:0.1) to buffer B (H₂O/CH₃CN/HCOOH, 5:95:0.05) over 10 min (flow rate: 1.0 mL/min) coupled to an Hewlett-Packard 1100 series mass spectrometer with an electrospray ionization source. LC-MS method B: HPLC-MS was recorded on an Agilent 1200 series system using an Xbridge RP C18 column (3.5 μm, 100 × 4.6 mm) with UV detection at 210, 254, and 280 nm. Mobile phase (MP) A: 0.2% HCOOH, 99.8% H₂O (v/v). Mobile phase B: 0.2% HCOOH, 99.8% MeCN (v/v). Flow rate: 1 mL/min. Gradient: 0–7 min, 0–90% MP B; 7–9 min, 90% MP B; 9–16 min, 10% MP B.

5-(Thiophen-2-yl)indoline-2,3-dione (20). 5-Iodoindoline-2,3-dione (13) (0.1 g, 0.36 mmol), thiophene-2-boronic acid pinacol ester (0.090 g, 0.43 mmol), and NaHCO₃ (0.06 g, 0.72 mmol) were dissolved in a mixture of DME/H₂O (5:1, 4.8 mL). The mixture was degassed with N₂ gas, after which Pd(dppf)Cl₂ (15 mg, 0.018 mmol) was added and the reaction vial was sealed and heated at 90 °C for 18 h. The crude reaction mixture was filtered over Celite and diluted with EtOAc, after which the organic layer was washed with a saturated NaHCO₃ solution. Organic layer was dried over MgSO₄, after which volatiles were evaporated under reduced pressure. The resulting crude solids were purified over SiO₂ using a gradient of 4:1 *n*-heptane/EtOAc toward 2:1 *n*-heptane/EtOAc, yielding 10 mg of the title compound (0.042 mmol, 12%). ¹H NMR (600 MHz, DMSO-*d*₆) δ 11.14 (s, 1H), 7.86 (dd, *J* = 8.2, 2.0 Hz, 1H), 7.75 (d, *J* = 2.0 Hz, 1H), 7.55–7.51 (m, 1H), 7.15–7.11 (m, 1H), 6.96 (d, *J* = 8.2 Hz, 1H). ¹³C NMR (101 MHz, DMSO-*d*₆) δ 184.63, 159.91, 150.11, 142.43, 135.43, 129.19, 129.05, 125.88, 124.11, 121.46, 118.92, 113.25. LC-MS (ESI) *m/z* calcd for C₁₂H₈NO₂S⁺, 230.26; found, 230.1 [M + H]⁺; *t*_R = 6.054 min.

Materials and [³H]GABA Uptake Assay. Ham's F12 nutrient mix, fetal bovine serum (FBS), penicillin–streptomycin, hygromycin B, trypsin, and Hank's balanced salt solution (HBSS, catalogue no. 14175-095) were purchased from Life Technologies (Paisley, UK). Plasmocin was obtained from InvivoGen (San Diego, CA, USA). Poly-D-lysine (PDL) and HEPES (4-(2-hydroxyethyl) piperazine-1-ethanesulfonic acid) were purchased from Sigma-Aldrich. [2,3-³H(N)]GABA (specific

radioactivity 35.0 Ci/mmol) and MicroScint-20 were purchased from PerkinElmer (Boston, MA, USA). GABA was purchased from Sigma-Aldrich (St. Louis, MO, USA). Isatin analogues 5–14 (see Table 1) were generously provided by 7TM Pharma, Denmark.

Cell Culture and GAT Expression. Generation and culture of the Chinese hamster ovary (CHO) Flp-in cell line stably expressing human GATs have been previously described.^{17,20}

[³H]GABA Uptake Assay and Compound Library Screening. The [³H]GABA competition uptake assay and kinetics studies were performed exactly as previously described using a 96-well format setup.²⁰

Data Analysis. Data and statistical analysis were performed in GraphPad Prism 6 (GraphPad Software, San Diego, CA, USA). Concentration–inhibition curves generated in the competition [³H]GABA uptake assay were fitted by nonlinear regression using the equation for sigmoidal concentration–response with variable slope: $Y = \text{bottom} + (\text{top} - \text{bottom}) / (1 + 10^{(\log(\text{IC}_{50} - X) \times \text{HillSlope})})$, where *Y* is the response, *X* is the logarithm of the concentration, top and bottom are the plateaus in same units as *Y*, and log IC₅₀ is the concentration giving a response half way between bottom and top. The HillSlope is the steepness of the curve. Concentration–inhibition curves were fitted to 100% inhibition by 3 mM GABA if the highest concentration of the inhibitor displayed less than 90% but more than 50% inhibition of [³H]GABA uptake. The IC₅₀ values of compounds displaying less than 50% but more than 10% inhibition were estimated as being greater than the highest tested concentration. Compounds showing less than 10% [³H]GABA uptake inhibition at the highest tested concentration were considered not to be active.

Data from kinetics experiments were analyzed using the Michaelis–Menten equation: $Y = V_{\text{max}} \times X / (K_m + X)$, where *Y* is the uptake velocity, *X* is substrate concentration, *V*_{max} is the maximum uptake velocity in the same units as *Y*, and *K*_m is the Michaelis–Menten constant in the same units as *X*.

Molecular Modeling. Models of hGAT1–3 and hBGT1 were constructed using Modeler 9.14, using the inward-facing, outward-occluded, and outward-open template structures of LeuT (PDB codes 3TT3, 2A65, 3F3A). Initial sequence alignment according to Beuming et al.²⁹ was further optimized in loop regions (see Supporting Information Figure S2). Crystal structures of MhsT and DAT_{cryst} were consulted for resolving secondary structural ambiguities. Two-hundred models for each transporter in all three conformations were generated and sorted according to DOPE score.

The Site Finder module of MOE 2014.09 was used for cavity analysis. Docking studies were carried out using the Schrödinger 2014.3 Suite. Structure preparation was performed with LigPrep, docking with the induced fit docking protocol. Isatin derivatives were drawn within MOE and prepared with LigPrep, sampled for a physiological pH range of 7.2 ± 0.2.

MD simulations were performed for 10 ns using Desmond 3.6 and the OPLS 2005 force field; *n* = 3 for hGAT1 and hGAT3. Protein models were placed in a POPC membrane that was manually adjusted after being set to TM residues and solvated using an SPC water model and 0.15 M NaCl. Trajectory analysis was carried out using VMD and Desmond's Simulation Interaction Diagram.

ASSOCIATED CONTENT

Supporting Information

Synthetic procedures for the synthesis of compounds 15–39 along with results and structures of the follow-up screening of 48 isatin analogues and molecular modeling data. The Supporting Information is available free of charge on the ACS Publications website at DOI: 10.1021/acschemneuro.5b00150.

AUTHOR INFORMATION

Corresponding Authors

* (P.W.) Phone: +45 39 17 98 11; E-mail: pw@sund.ku.dk.

* (R.P.C.) Phone: +45 35 33 65 66; E-mail: rac@sund.ku.dk.

Funding

This work was supported by the Lundbeck Foundation, the Novo Nordisk Foundation, the A.P. Møller Foundation for the Advancement of Medical Sciences, and the Drug Research Academy.

Notes

The authors declare no competing financial interest.

ABBREVIATIONS

BGT1, betaine-GABA transporter; CHO, chinese hamster ovary; CNS, central nervous system; GABA, γ -aminobutyric acid; GAT, GABA transporter; SAR, structure–activity relationship; (S)-SNAP 5114, 1-[2-[tris(4-methoxyphenyl)methoxy]ethyl]-(S)-3-piperidinecarboxylic acid; TM, transmembrane

REFERENCES

- (1) Rowley, N. M., Madsen, K. K., Schousboe, A., and Steve White, H. (2012) Glutamate and GABA synthesis, release, transport and metabolism as targets for seizure control. *Neurochem. Int.* 61, 546–558.
- (2) Meldrum, B. S., and Chapman, A. G. (1999) Basic Mechanisms of Gabitril (Tiagabine) and Future Potential Developments. *Epilepsia* 40, S2–S6.
- (3) Nielsen, E. B., Suzdak, P. D., Andersen, K. E., Knutsen, L. J., Sonnewald, U., and Braestrup, C. (1991) Characterization of tiagabine (NO-328), a new potent and selective GABA uptake inhibitor. *Eur. J. Pharmacol.* 196, 257–266.
- (4) Madsen, K. K., White, H. S., and Schousboe, A. (2010) Neuronal and non-neuronal GABA transporters as targets for antiepileptic drugs. *Pharmacol. Ther.* 125, 394–401.
- (5) Borden, L. A. (1996) GABA transporter heterogeneity: pharmacology and cellular localization. *Neurochem. Int.* 29, 335–356.
- (6) Lehre, A. C., Rowley, N. M., Zhou, Y., Holmseth, S., Guo, C., Holen, T., Hua, R., Laake, P., Olofsson, A. M., Poblete-Naredo, I., Rusakov, D. A., Madsen, K. K., Clausen, R. P., Schousboe, A., White, H. S., and Danbolt, N. C. (2011) Deletion of the betaine-GABA transporter (BGT1; slc6a12) gene does not affect seizure thresholds of adult mice. *Epilepsy Res.* 95, 70–81.
- (7) White, H. S., Watson, W. P., Hansen, S. L., Slough, S., Perregaard, J., Sarup, A., Bolvig, T., Petersen, G., Larsson, O. M., Clausen, R. P., Frølund, B., Falch, E., Krogsgaard-Larsen, P., and Schousboe, A. (2004) First demonstration of a functional role for central nervous system betaine/ γ -aminobutyric acid transporter (mGAT2) based on synergistic anticonvulsant action among inhibitors of mGAT1 and mGAT2. *J. Pharmacol. Exp. Ther.* 312, 866–874.
- (8) Madsen, K. K., Ebert, B., Clausen, R. P., Krogsgaard-Larsen, P., Schousboe, A., and White, H. S. (2011) Selective GABA transporter inhibitors tiagabine and EF1502 exhibit mechanistic differences in their ability to modulate the ataxia and anticonvulsant action of the extrasynaptic GABA(A) receptor agonist gaboxadol. *J. Pharmacol. Exp. Ther.* 338, 214–219.
- (9) Clarkson, A. N., Huang, B. S., Macisaac, S. E., Mody, I., and Carmichael, S. T. (2010) Reducing excessive GABA-mediated tonic inhibition promotes functional recovery after stroke. *Nature* 468, 305–309.
- (10) Melone, M., Cozzi, A., Pellegrini-Giampietro, D. E., and Conti, F. (2003) Transient focal ischemia triggers neuronal expression of GAT-3 in the rat perilesional cortex. *Neurobiol. Dis.* 14, 120–132.
- (11) Pozdnyakova, N., Dudarenko, M., Yatsenko, L., Himmelreich, N., Krupko, O., and Borisova, T. (2014) Perinatal hypoxia: different effects of the inhibitors of GABA transporters GAT1 and GAT3 on the initial velocity of [^3H]GABA uptake by cortical, hippocampal, and thalamic nerve terminals. *Croat. Med. J.* 55, 250–258.
- (12) Pabel, J., Faust, M., Prehn, C., Worlein, B., Allmendinger, L., Hofner, G., and Wanner, K. T. (2012) Development of an (S)-1-[2-[tris(4-methoxyphenyl)methoxy]ethyl]piperidine-3-carboxylic acid [(S)-SNAP-5114] carba analogue inhibitor for murine gamma-aminobutyric acid transporter type 4. *ChemMedChem* 7, 1245–1255.
- (13) Dalby, N. O. (2000) GABA-level increasing and anticonvulsant effects of three different GABA uptake inhibitors. *Neuropharmacology* 39, 2399–2407.
- (14) Kristensen, A. S., Andersen, J., Jorgensen, T. N., Sorensen, L., Eriksen, J., Loland, C. J., Stromgaard, K., and Gether, U. (2011) SLC6 neurotransmitter transporters: structure, function, and regulation. *Pharmacol. Rev.* 63, 585–640.
- (15) Reyes, N., and Tavoulari, S. (2011) To be, or not to be two sites: that is the question about LeuT substrate binding. *J. Gen. Physiol.* 138, 467–471.
- (16) Quick, M., Shi, L., Zehnpfennig, B., Weinstein, H., and Javitch, J. A. (2012) Experimental conditions can obscure the second high-affinity site in LeuT. *Nat. Struct. Mol. Biol.* 19, 207–211.
- (17) Kragholm, B., Kvist, T., Madsen, K. K., Jorgensen, L., Vogensen, S. B., Schousboe, A., Clausen, R. P., Jensen, A. A., and Brauner-Osborne, H. (2013) Discovery of a subtype selective inhibitor of the human betaine/GABA transporter 1 (BGT-1) with a non-competitive pharmacological profile. *Biochem. Pharmacol.* 86, 521–528.
- (18) Yamashita, A., Singh, S. K., Kawate, T., Jin, Y., and Gouaux, E. (2005) Crystal structure of a bacterial homologue of Na⁺/Cl⁻-dependent neurotransmitter transporters. *Nature* 437, 215–223.
- (19) Penmatsa, A., Wang, K. H., and Gouaux, E. (2013) X-ray structure of dopamine transporter elucidates antidepressant mechanism. *Nature* 503, 85–90.
- (20) Al-Khawaja, A., Petersen, J. G., Damgaard, M., Jensen, M. H., Vogensen, S. B., Lie, M. E., Kragholm, B., Bräuner-Osborne, H., Clausen, R. P., Frølund, B., and Wellendorph, P. (2014) Pharmacological identification of a guanidine-containing beta-alanine analogue with low micromolar potency and selectivity for the betaine/GABA transporter 1 (BGT1). *Neurochem. Res.* 39, 1988–1996.
- (21) Sandmeyer, T. (1919) Über Isonitrosoacetanilide und deren Kondensation zu Isatinen. *Helv. Chim. Acta* 2, 234–242.
- (22) Miyaura, N., and Suzuki, A. (1995) Palladium-Catalyzed Cross-Coupling Reactions of Organoboron Compounds. *Chem. Rev.* 95, 2457–2483.
- (23) Gérard, A. L., Lisowski, V., and Rault, S. (2005) Direct synthesis of new arylanthranilic acids via a Suzuki cross-coupling reaction from iodoisatins. *Tetrahedron* 61, 6082–6087.
- (24) Liu, Y. C., Ye, C. J., Chen, Q., and Yang, G. F. (2013) Efficient synthesis of bulky 4-substituted-isatins via microwave-promoted Suzuki cross-coupling reaction. *Tetrahedron Lett.* 54, 949–955.
- (25) Wang, C. H., White, A. R., Schwartz, S. N., Alluri, S., Cattabiani, T. M., Zhang, L. K., Chan, T. M., Buevich, A. V., and Ganguly, A. K. (2012) Novel synthesis and functionalization of ortho–ortho disubstituted biphenyls and a highly condensed novel heterocycle using radical cyclization reaction. *Tetrahedron* 68, 9750–9762.
- (26) Ananthan, S., Saini, S. K., Khare, R., Clayton, S. D., Dersch, C. M., and Rothman, R. B. (2002) Identification of a novel partial inhibitor of dopamine transporter among 4-substituted 2-phenylquinazolines. *Bioorg. Med. Chem. Lett.* 12, 2225–2228.
- (27) Lee, F. J., Pristupa, Z. B., Ciliax, B. J., Levey, A. I., and Niznik, H. B. (1996) The dopamine transporter carboxyl-terminal tail. Truncation/substitution mutants selectively confer high affinity dopamine uptake while attenuating recognition of the ligand binding domain. *J. Biol. Chem.* 271, 20885–20894.
- (28) Scholze, P., Freissmuth, M., and Sitte, H. H. (2002) Mutations within an intramembrane leucine heptad repeat disrupt oligomer formation of the rat GABA transporter 1. *J. Biol. Chem.* 277, 43682–43690.
- (29) Beuming, T., Shi, L., Javitch, J. A., and Weinstein, H. (2006) A comprehensive structure-based alignment of prokaryotic and eukaryotic neurotransmitter/Na⁺ symporters (NSS) aids in the use of the LeuT structure to probe NSS structure and function. *Mol. Pharmacol.* 70, 1630–1642.